Cathode-Erosion Numerical Model with Two-Dimensional Cylindrical Symmetry for Magnetoplasmadynamic Thrusters

Thada Suksila

Advanced Propulsions and Rockets Lab
Department of Mechanical and Aerospace Engineering, Faculty of Engineering
King Mongkut's University of Technology North Bangkok,
1518 Pracharat Sai I Rd. Wongsawang, Bangsue, Bangkok 10800, Thailand.
thada.s@eng.kmutnb.ac.th, Mobile: 0963519519, Fax: 025869541

Abstract

Magnetoplasmadynamic (MPD) thrusters are considered as among the primary candidates for electrical thrusters used in interplanetary missions. An MPD thruster mainly consists of a cathode, an anode, plasma, and a cathode–plasma interaction. The cathode and anode must operate and remain in very high temperature for a long-duration mission. However, a problem arises in that cathode erosion occurs, especially at the cathode surface, due to the cathode–plasma interaction. Therefore, cathode erosion is a major problem in MPD thrusters. Fundamental knowledge of the cathode-erosion process is not entirely complete because of the nonlinearity and complexity of the cathode–plasma interactions. This study mainly focuses on improving the two-dimensional (2D) cylindrical symmetry cathode-erosion model to predict the cathode mass loss from the start until a steady-state condition is reached. Two-dimensional cylindrical symmetry cathode-erosion model meshes were generated using a non-uniform triangular-mesh technique. In addition, the cathode–plasma interaction was included at the cathode surface as a thin layer at the surface. Then, the cathode temperature was solved using a nonlinear heat-diffusion equation, and the cathode-erosion mass loss was determined from the cathode evaporation rate, which depends on the cathode temperature. The results show that the cathode-erosion mass loss strongly depends on the cathode temperature and current density. However, the pressure exerts only a small effect. The numerical data were compared with the experimental data and showed only a small discrepancy in the cathode-erosion mass loss. This 2D cylindrical symmetry cathode-erosion model can help in the development of future MPD thrusters to predict the duration of a mission.

Keywords: Magnetoplasmadynamic (MPD), Cathode erosion, Cathode–plasma simulation, 2D cylindrical symmetry cathode-erosion model

1. Introduction

A magnetoplasmadynamic (MPD) thruster is an electric thruster that can potentially be used in spacecrafts to carry human and scientific instruments to deep space for a long-journey mission owing to its high fuel efficiency and high specific impulse (I_{sp}) [1-5]. The anodes (+) are connected to a high-voltage and high-current power supply with small gap between them, as shown in Fig. 1. At the cathode base, inert gas, usually argon, is injected through this gap and passes through the anode. Argon is heated up until its electron outer shell reaches the first ionization energy level. At this point, two main particles exist in the flow: positive argon and electron.

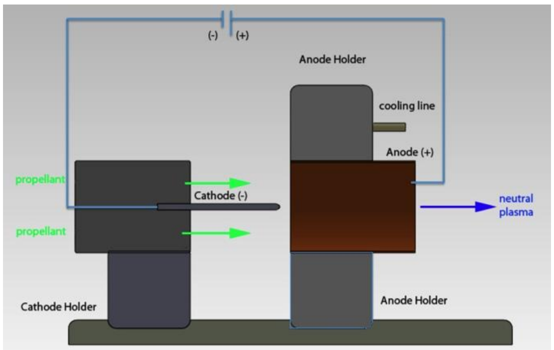

Fig. 1 Section side view of a solid cathode assembly.

This electron and positive argon are collectively called argon plasma. This argon plasma interacts with the electromagnetic field that surrounds the cathode and the electrical current field lines. Then, a thrust force is created from the Lorentz force [1], as shown in Fig. 2.

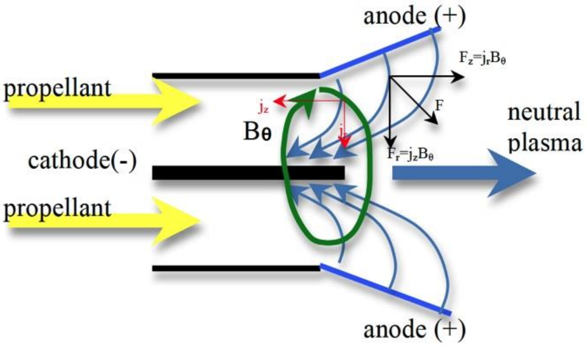

Fig. 2 Current density and magnetic field that creates a thrust force (*F*).

Typically, a cooling system is installed for the anode when the temperature reaches 1500–2000 K. MPD thrusters operate in pressure of approximately 60–100 Pa. [2-4]. A laboratory experimental MPD thruster assembly in a pressure chamber is shown in Fig. 3.

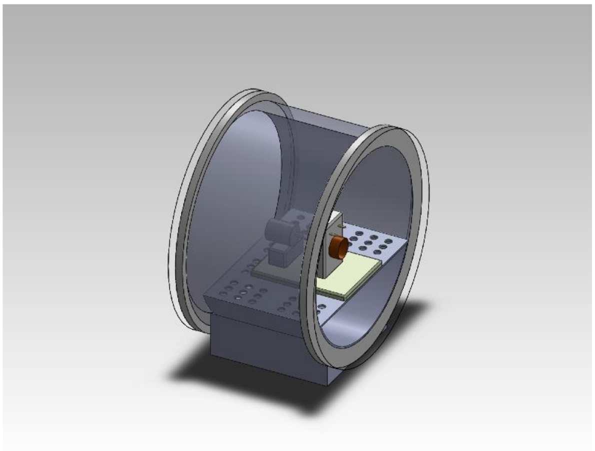

Fig. 3 Solid cathode assembly in the pressure chamber.

2. NUMERICAL MODELS

2.1 Introduction

In recent years, the advancements in graphics and processor technology have allowed computational simulations to solve nonlinearity problems owing to their accuracy and sophistication. In addition, they offer several benefits, e.g., they allow scientists and researchers to observe how the systems respond. Further, they can help detect erroneous design calculation before developing and building an experimental setup, which can save a great deal of money.

In 1992, Niewood et al. developed a quasi-one-dimensional (1D) model of an MPD thruster that included a two-fluid flow [6]. In 1996, Hulston et al. conducted a 1D numerical simulation of cathode thermal erosion [7]. In 1996, Goodfellow conducted an experiment and created a quasi-1D numerical model. This model required thermal and near-cathode plasma models in a steady state for an electrical thruster to predict the lifetime of the cathode [2]. Rossignal et al. introduced a 1D model of a cathode sheath in an electrical arc; however, the thermal and electrical conductivity values were constant [8].

In the current study, a two-dimensional (2D) cylindrical symmetry cathode numerical model that includes the cathode–plasma interaction (plasma sheath) and the temperature-dependent electrical and thermal conductivity parameters is investigated. However, the magnetic field is not included. The MPD thruster has several domains: cathode, anode, and plasma, as shown in Fig. 4.

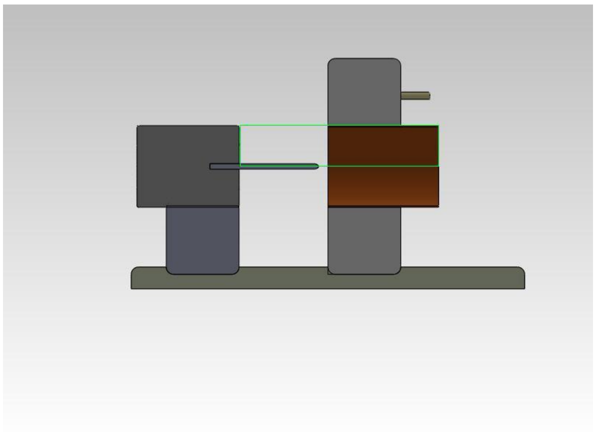

Fig. 4 Boundary of the 2D cylindrical symmetry MPD thruster simulation.

2.2 Computational meshes

The computational meshes in this study were developed using the triangular computational-grid method [9]. In other words, this grid is topologically equivalent to an equilateral-triangle array where six triangles meet at every interior mesh point. The primary triangle mesh has a common vertex and a secondary mesh with 12-sided figures whose vertices are alternately the centroids of six adjacent triangles and midpoints of six adjacent sides, as shown in Fig. 5.

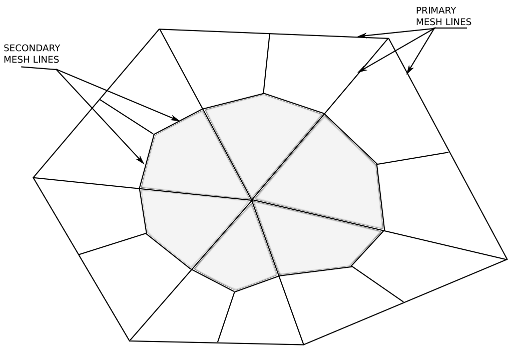

Fig. 5 Primary and secondary mesh lines [1].

The main advantages of using the structured triangular grids rather than the rectangular structural grids are that they can be easily fitted into the irregular shape of the boundary domain and can be used with the adaptive method to confine the grid in a specific region.

The Cartesian coordinate is introduced, and it can be applied to the boundary of this 2D cylindrical symmetry cathode-erosion numerical model. The nonlinear diffusion equation can be expressed as

$$c\frac{\partial\emptyset}{\partial t} = \nabla\cdot(\lambda\nabla\phi) + S. \tag{1}$$

The generalized Poisson equation for steady state can be expressed as

$$\nabla\cdot(\lambda\nabla\emptyset) + S = 0 \tag{2}$$

where c is the heat capacity, S is the function of the position or source term (i.e., thermionic heating), $\emptyset$ is the temperature, potential, or voltage at the vertices of the triangle, and λ is a function of $\emptyset$ or its derivatives (electrical or thermal conductivity). Then, we solve the numerical Laplace equation to construct the non-uniform triangle meshes [9-11].

2.4 Outline of the Algorithm

In this section, the details of the 2D cylindrical symmetry cathode-erosion numerical model are described in several steps as follows:

1. Fig. 6 shows that the physical grid space is separated into three main regions, namely, the cathode, anode, and cathode-plasma interaction. The number of cells in the computational grid space can be specified, as shown in Fig. 7.

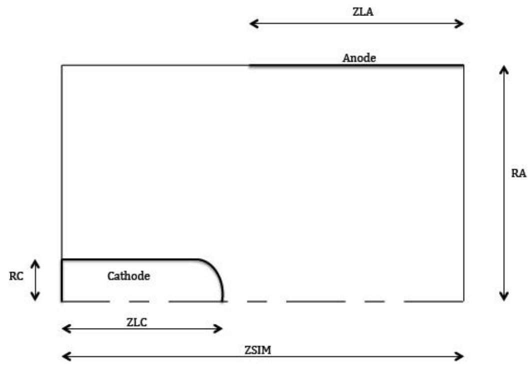

Fig. 6 Physical grid space with the physical dimension designated as R_c, R_A, Z_{sim}, Z_{LC}, and Z_{LA}.

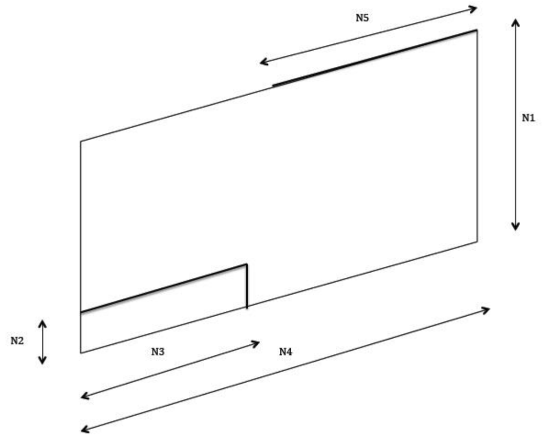

Fig. 7 Computational grid space with the number of cells designated as N_1, N_2, N_3, N_4, and N_5.

2. R_A, R_C, Z_{LC}, Z_{SIM}, and Z_{LA} denote the anode radius, cathode radius, cathode length, MPD system length, and anode length, respectively. The values are 27, 1.98, 75, 157, and 76 mm, respectively.

3. Fig. 7 shows that N_1, N_2, N_3, N_4, and N_5 denote the number of cells at the anode radius, cathode radius, cathode length, MPD system length, and anode length, respectively.

4. The program generates the computational and physical grid spaces shown in Figs. 6 and 7.

5. Each point is saved in a hexagonal grid point, and each point has a coordinate value in both the computational and physical grid spaces.

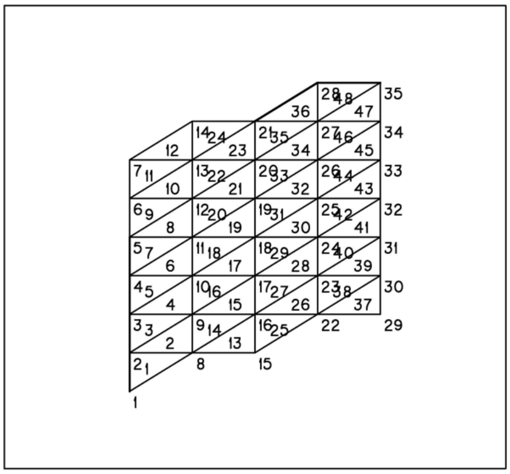

Fig. 8 Computational grid space $N_1 = 6$, $N_2 = 4$, $N_3 = 2$, $N_4 = 4$, and $N_5 = 2$.

6. Two triangle types exist. The first type is denoted by triangle numbers 1, 3, 5, 7, 9, 11, 14, and 16, etc. The second type is denoted by 2, 4, 6, 8, 10, 12, 13, and 15, etc., as shown in Fig. 8.

7. The computational and physical grids are solved. For the physical grids, additional numerical methods are required to solve the Laplace equation, i.e., "lower–upper decomposition" and "backward substitutions."

8. The output can be plotted by any plotting software, as shown in Figs. 8 and 9, using different values of N_1, N_2, N_3, N_4, and N_5.

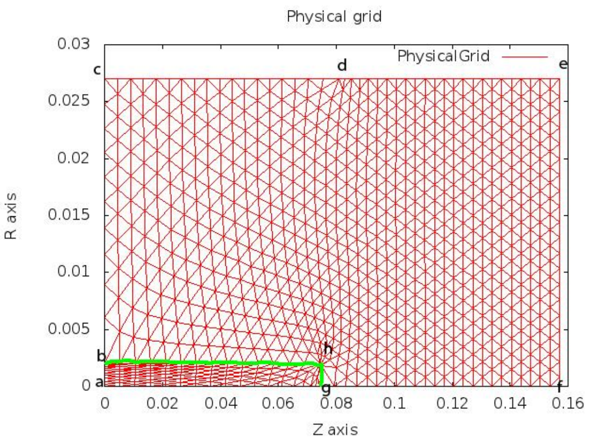

Fig. 9 Physical grid space $N_1 = 20$, $N_2 = 10$, $N_3 = 18$, $N_4 = 42$, and $N_5 = 24$ (the cathode-plasma interaction applied on the cathode surface).

2.5 Boundary conditions

At the base of the cathode, the temperature is fixed at T_{base} or T_0 with a typical value of 500 or 1500 K [2-5]. An alternative boundary condition can be specified as needed for comparison with the experimental data. At the anode, the simplest condition is to set plasma temperature T_{pA} to a fixed value in which a typical value is chosen under the condition that the degree of ionization obtained by the Saha equation be 10^{-2} to 10^{-1} [2-4] (an alternative boundary condition obtained to analyze the experimental data). Plasma pressure P is considered constant in which the typical value is 0.5 Torr (66 Pa). The current and potential boundary conditions are described in [3].

2.5 Cathode–plasma-interaction region

The characteristic of the near-cathode model represents the characteristic between the plasma and cathode in steady state and considers the sheath to be a discontinuity between the cathode and plasma. The model predicts the heat flux, current density, electron-number density, and electron temperature (eV) as a function of temperature and pressure at the near-cathode surface. The cathode–plasma interaction or plasma sheath is applied at the cathode surface using the developed numerical model [2].

2.6 Heat capacity and electrical and thermal conductivity values

For the 2D cylindrical symmetry cathode-erosion numerical model, the electrical conductivity, thermal conductivity, and heat capacity, which are temperature and pressure dependent, are applied. However, in this work, the pressure is fixed at 66 Pa only but can be adjusted as needed.

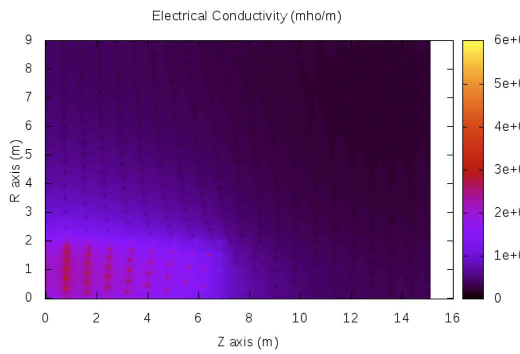

Fig. 10 Electrical conductivity distribution in the

cathode and plasma regions in the MPD thruster.

The electrical conductivity of argon plasma significantly changes as the temperature changes [12, 13].

This temperature dependence must be included in the investigation to fully perform realistic MPD thruster simulations. The values of the electrical conductivity, thermal conductivity, and heat capacity are shown in Figs. 10–12, respectively.

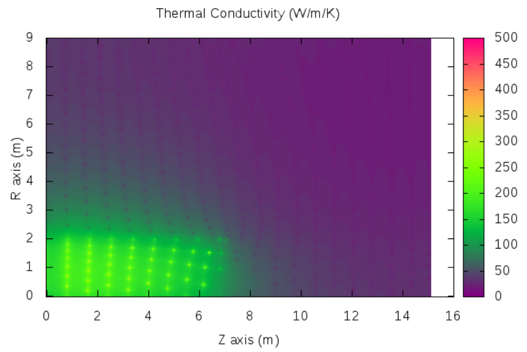

Fig. 11 Thermal conductivity distribution of the cathode and plasma regions in the MPD thruster.

The parameters are set as follows: L_C = 7.5 m, L_A = 7.6 m, R_C = 2.0 m, R_A = 9.0 m, $T_{c,\mathrm{init}}$ = 3300 K, $T_{e,\mathrm{init}}$ = 9000 K, V_{init} = 100 V, and I = 100 A. N_1 = 24, N_2 = 8, N_3 = 10, N_4 = 20, and N_5 = 8. However, some of these parameters can be changed as needed to determine how an MPD thruster system responds.

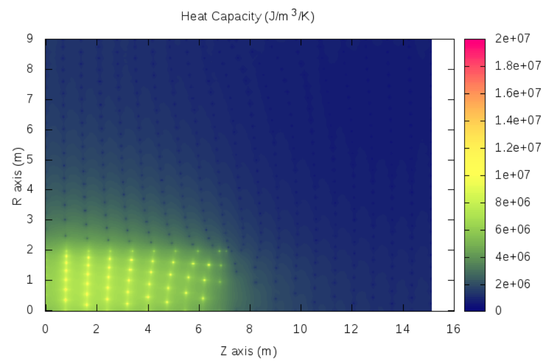

Fig. 12 Heat capacity distribution in the cathode and plasma region in the MPD thruster.

2.7 Cathode-erosion rate values

The cathode- erosion rate values strongly depend on the temperature; the higher the temperature is, the more the erosion rate increases. The details are explained in [2]–[4].

3. Fully combined cathode and plasma regions in the cathode–plasma-interaction model in the 2D cylindrical symmetry cathode-erosion model

The nonlinear heat-diffusion equation in the cylindrical coordinate must be solved to obtain the temperature in the system. Equation (1) can be expressed as

$$C_p(T)\frac{\partial T}{\partial t} = \frac{1}{r}\nabla\cdot(rK(T)\nabla T) + S \tag{3}$$

where S is the function of the position or source term (i.e., thermionic heating), T is the temperature at the vertex of the triangle, $K(T)$ is the temperature that depends on the thermal conductivity, and $C_p(T)$ is the temperature that depends on the heat capacity. At steady state, Eq. (3) can be expressed as

$$\nabla\cdot(rK(T)\nabla T) + S = 0. \tag{4}$$

Equation (3) can be expressed in finite-difference approximation as

$$\frac{\Delta T}{\Delta t} = \frac{1}{G}\left[\sum_{i=1}^{6} w_i(T_i - T) + S\right] \tag{5}$$

$$G = \sum_{i=1}^{6} c_p(T)_{i+1/2}\bar{\bar{r}}_{i+1/2}a_{i+1/2}, \tag{6}$$

$$S = \sum_{i=1}^{6} j_{i+1/2}\bar{\bar{r}}_{i+1/2}a_{i+1/2}, \tag{7}$$

$$\sum_{i=1}^{6} w_i = \frac{1}{4}\sum_i \frac{K(T)_{i+1/2}}{A_{i+1/2}}\bar{\bar{r}}_{i+1/2}(S_{i+1} - S_i)^2, \tag{8}$$

$$\bar{\bar{r}}_{i+\frac{1}{2}} = \frac{7}{12}\bar{r}_{i+1/2} + \frac{5}{12}r, \tag{9}$$

$$\bar{r}_{i+1/2} = \frac{1}{3}(r + r_i + r_{i+1}), \tag{10}$$

where i is the number of triangles at the vertices, i.e., 1 to 6, or the vertex. $A_{i+1/2}$ is the area of the triangle, $a_{i+1/2}$ is one-third of the area of the triangle (shaded area in Fig. 5), $j_{i+1/2}$ is the current density, r is the radius of the triangle from the center line, $\bar{r}_{i+1/2}$ is the average radius of the triangle, i + 1/2, $\bar{\bar{r}}_{i+\frac{1}{2}}$ is the average radius of the quadrilateral at vertex r, and w_i is a coupling coefficient. Using the difference of the first derivative with respect to time, which has a first-order approximation, the equations can be expressed as

$$\frac{\Delta T_i}{\Delta t} = \frac{T_i^{n+1} - T_i^n}{\Delta t} \quad (11)$$

Rearranging Eq. (11) yields

$$T_i^{n+1} = T_i^n + \frac{\Delta t}{G}\left[\sum_{i=1}^{6} w_i\,(T_i - T) + S\right]. \quad (12)$$

The included cathode–plasma interaction at the cathode surface and the plasma next to the cathode surface can be expressed as

$$T_{NC}^{n+1} = T_{NC}^n + \frac{\Delta t}{G}\left[\sum_{i=1}^{6} w_i (T_i - T) + S + \dot{Q} a_{i+1/2}\right] \quad (13)$$

$$T_{NC+1}^{n+1} = T_{NC+1}^n + \frac{\Delta t}{G}\left[\sum_{i=1}^{6} w_i (T_i - T) + S - \dot{Q} a_{i+1/2}\right] \quad (14)$$

where n is the time step and T_{NC} and T_{NC+1} are the temperatures at the cathode surface and at the plasma next to the cathode surface, respectively. The heat transfer is defined as $\dot{Q}$ for heating the cathode and $-\dot{Q}$ for cooling the cathode [2, 3].

4. Critical time increment of the 2D cylindrical symmetry cathode-erosion numerical model

The von Neumann criterion can be applied to Eqs. (12)–(14) for stability of the system.

$$\Delta t \le \frac{G}{2\sum_{i=1}^{6} w_i} \quad (15)$$

However, the other criterion, i.e., ohmic heating, must be satisfied in order for the system to also achieve stability.

$$\Delta t \le \frac{G}{2S} \quad (16)$$

In addition, the heat-flux cathode–plasma criterion at the cathode surface and plasma next to the cathode surface must be considered.

$$\Delta t \le \frac{G}{2\dot{Q} a_{i+1/2}} \quad (17)$$

From the above equations, we can see that the von Neumann criterion is composed of the thermal conductivity and the heat capacity terms. However, the ohmic-heating criterion is related to the current density and the heat-capacity terms. At the cathode surface, the heat-flux cathode–plasma criterion is related to the heat capacity, heat flux, and area of the cells.

5. Numerical results of the 2D cylindrical symmetry cathode-erosion model

The cathode evaporation mass loss of the 2D cylindrical symmetry model strongly depends on the current density, as shown in Fig. 13.

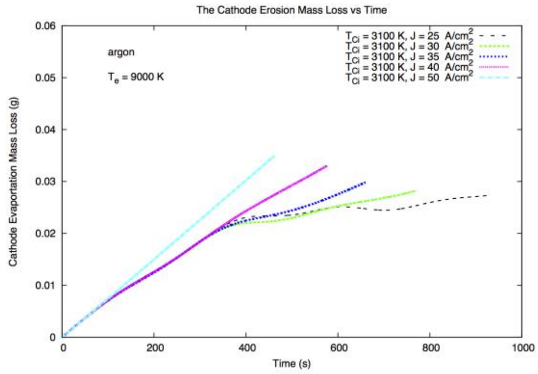

Fig. 13 Cathode evaporation mass loss as a function of time and current density.

The time to reach steady state is approximately 10–20 min [2-4]. However, the pressure slightly affects the cathode evaporation mass loss, and the time to reach steady state decreases as the pressure decreases, as shown in Fig. 14.

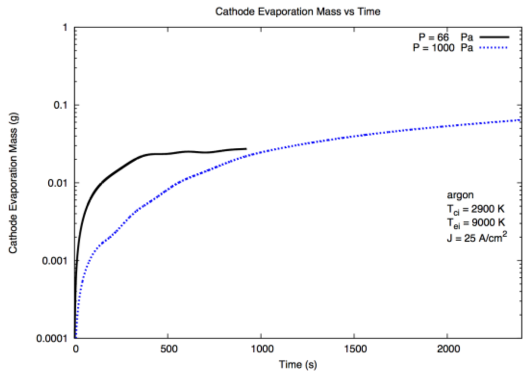

Fig. 14 Cathode evaporation mass loss as a function of time and pressure.

6. Comparison of numerical and experimental results

The results of the 2D cylindrical symmetry cathode-erosion numerical model were compared with the experimental results [2-4]. This 2D model predicted that the cathode evaporation mass loss will have a similar trend to that of the experiments from the start to below 300 s, as shown in Fig. 15. However, beyond 300 s, the 2D model estimated loss is approximately 0. 05 g, whereas the experiments show only a 0.04-g loss. As a result, the 2D model over predicted around 25%.

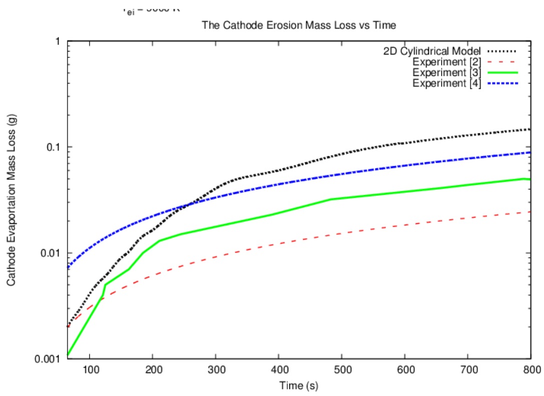

Fig. 15 Comparison of the 2D cylindrical symmetry cathode-erosion numerical model data with the experimental data.

The result of the 2D model was also compared with those of the other numerical models. The quasi-2D cathode-erosion model at $j = 25$ and 50 A/cm^2 estimated the cathode-erosion mass loss as 0.015 and 0.08 g, respectively, at 300 s. The 2D cylindrical model predicted a 0.03-g loss at $j = 50$ A/cm^2 in 300 s.

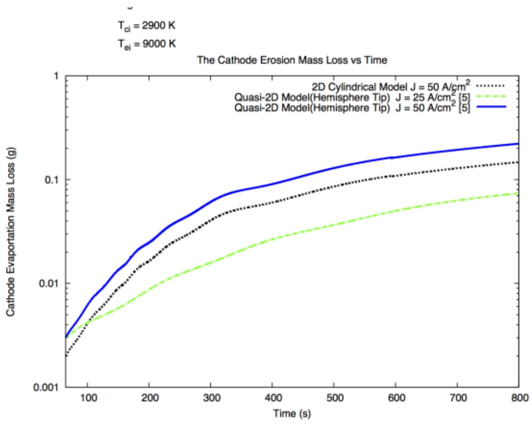

Fig. 16 Comparison of the 2D cylindrical symmetry cathode-erosion numerical model results with the quasi-2D model [5].

Fig. 16 shows the comparison between the 2D cylindrical model with the quasi-2D model [5] at various current densities. The resulting data show that the 2D cylindrical model estimated a higher cathode erosion because the 2D cylindrical model includes a more sophisticated area that the quasi-2D could not have achieved.

7. Conclusion

The objective of this study is to improve the 2D cylindrical symmetry cathode- erosion numerical model reported in the literature using cathode temperature to predict the cathode evaporation mass loss in MPD thrusters. The 2D cathode-erosion model can predict the upper limits of cathode evaporation mass loss according to the experimental data. However, when compared with the quasi- 2D model, the 2D cylindrical model estimated a lower cathode-erosion mass loss. Thus, this study successfully developed numerical models of cathode erosion that can predict the cathode-erosion mass loss. These models can be applied in the development of MPD thrusters for future application. However, this 2D cylindrical model did not fully include the effect of magnetic-field relationships, which need to be explored in future studies. Some additional materials for MPD thrusters can be found in [14]–[22].

8. References

[1] Jahn, R. G. and von Jaskowsky, W. (1968). Physics of electric propulsion, vol. 288. McGraw-Hill.

[2] Goodfellow, K. D. (1996). A theoretical and experimental investigation of cathode processes in electric thrusters, Ph.D. Dissertation, Aerospace Engineering Dept., Univ. of Southern California, 42–91 and 272–276.

[3] Codron, D. A. and Erwin, D. (2012). Experimental studies on high current arc discharges for magnetoplasmadynamic thrusters, in *Aerospace Conference, 2012 IEEE, IEEE*.

[4] Schrade, H. O., Auweter-Kurtz, M., and Kurtz,

H. L. (1985). Cathode erosion studies on MPD-thrusters, *American Institute of Aeronautics and Astronautics, Inc.*, 1–9.

[5] Suksila, T. (2016). Numerical models of cathode erosion for magnetoplasmadynamic thrusters, *International Journal of Applied Engineering Research* 11, vol. 23, 11266–11272.

[6] Niewood, E. and Martinez-Sanchez, M. (1992). Quasi-one-dimensional numerical simulation of magnetoplasmadynamic thrusters, *Journal of Propulsion and Power*, vol. 8, no. 5.

[7] Hulston, C. K. J., Redlich, P. J., Jackson, W. R., Marshall, M., Larkins, F. P., Mehta, R. C., Andrews, S., and Ramachandran, P. V. (1996). Thermal erosion of magnetoplasmadynamic thruster cathode, *International Journal of Heat and Mass Transfer*, vol. 39, no. 8.

[8] Rossignol, J., Clain, S., and Abbaoui, M. (2003). The modelling of the cathode sheath of an electrical arc in vacuum, *Journal of Physics D: Applied Physics*, vol. 36, 1495.

[9] Winslow, A. M. (1966). Numerical solution of the quasilinear Poisson equation in a nonuniform triangle mesh, *Journal of Computational Physics*, vol. 1, no. 2.

[10] Hoffman, K. A. and Chiang, S. T. (2000). Computational fluid dynamics—Volume II, *Engineering Education System*.

[11] Hoffman, K. A. (1989). Computational fluid dynamics for engineers, Austin, TX: *Engineering Education System*.

[12] Ahtye, W. F. (1965). A critical evaluation of methods for calculating transport coefficients of partially and fully ionized gases, *National Aeronautics and Space Administration*.

[13] Suksila, T. (2015). 1D and quasi-2D numerical models of the cathode temperature in steady-state magnetoplasmadynamic thrusters, *International Journal of Applied Engineering Research* 10 vol. 18, 38714–38719.

[14] Humble, R. W., Henry, G. N., Larson, W. J., U.S. Defense, U.S. Aeronautics and S. Administration (1995). Space propulsion analysis and design, McGraw-Hill.

[15] Sutton, G. P. and Biblarz, O. (2011). Rocket propulsion elements, Wiley.

[16] Mattingly, J. D. and von Ohain, H. (2006). Elements of propulsion: Gas turbines and rockets, *American Institute of Aeronautics and Astronautics*.

[17] Friedensen, V. P. (1998). Space nuclear power: Technology, policy, and risk considerations in human missions to Mars, *Acta Astronautica*, vol. 42, no. 1-8.

[18] Mikellides, P. G. (2004). Modeling and analysis of a megawatt- class magnetoplasmadynamic thruster, *Journal of Propulsion and Power*, vol. 20, no. 2.

[19] Toki, K., Shimizu, Y., and Kuriki, K. (1986) Application of MPD thruster systems to interplanetary missions, *Journal of Propulsion and Power*, vol. 2.

[20] Sasoh, A., Solem, A., and Arakawa, Y. (1988). 10 kW steady- state MPD thruster, Tokyo, University, Faculty of Engineering, *Journal, Series B*, vol. 39.

[21] Polk, J. E. (1996). Mechanisms of cathode erosion in plasma thrusters, PhD thesis, Princeton University.

[22] Boulos, M. I., Fauchais, P., and Pfender, E. (1994). Thermal plasmas: Fundamentals and applications, vol. 1. Springer.